Large-Eddy Simulation in the vicinity of the RAF-6E airfoil in a reduced domain

László Nagy, Tamás Régert, Máté Márton Lohász

Budapest University of Technology and Economics (BME), Department of Fluid Mechanics

nagy@ara.bme.hu

Abstract

Large-eddy simulation using dynamic Smagorinsky Sub-Grid Scale model was performed to investigate the flow past an airfoil at an angle of attack of 5° at chord Reynolds number of 122000. The simulations were carried out using the incompressible implicit second-order finite volume method with a collocated variable arrangement implemented in ANSYS-FLUENT commercial code. Different computational grids were used both in terms of spanwise size and spanwise grid resolution to investigate its effect on the integral and instantaneous properties of the flow. The simulation scenarios were established in the aspect of the different smallest spanwise domain and finest grid shown the best results compare the measurements moreover 7 flow through number is enough to prepare comparison. Streamwise velocity components and velocity fluctuations of these numerical simulations were compared with Laser Doppler Anemometry measurements.

1. Motivation of this research activity

The fan is a frequently used mechanical device used in air-condition system, such as in buildings and traffic vehicles. A parameter with growing importance is the fan noise level. The academic version of the fan in confined flow could be a sole airfoil.

Half decade ago RAF-6E airfoil wind tunnel measurements were carried out in the Theodore von Kármán Wind Tunnel Laboratory (WTL) National Physics Laboratory (NPL) wind tunnel of BME Department of Fluid Mechanics (DFM). Applied these Laser Doppler Anemometry (LDA) and static pressure on the airfoil measurements data the large-eddy simulation (LES) on airfoil research has began in frame of an extensive reduction of aerodynamic noise of axial flow fans. The methodology of the noise prediction fan is based on the so called hybrid method which has two well separated steps.

- First: The unsteady, three-dimensional and incompressible aerodynamic flow field is computed using LES.
- Second: The unsteady pressure fluctuation on the surface(s) are extracted from the first step to be post-processed in an acoustic solver.

In this frame of the research LES in the vicinity of the RAF-6E airfoil results are summarized in this article.

Regarding the velocity in the wind tunnel, it is a low-speed axial fan. The Reynolds number based on the chord *(c)*, inlet reference velocity (U_{ref}) and kinematic viscosity (ν) was 122 000. The blockage of wing at this 5° angle of attack is 7.5% in test cross section of NPL. The wind tunnel has a cross section of 500 x $500mm$. An ILA flowPOINT fp50-fus LDA system has been connected to the test section. The pressure measurements were performed with a Betz-type manometry. Results of smoke with laser sheet and oil flow visualization confirmed that the flow at the midspan can be handled as two-dimensional, i.e. a wide spanwise region in the middle of the test section exists, where no effect of the side wall could be recognized. At the measurement conditions the Mach number was 0.03.

2. Introduction

Present paper deals with a key problem of state-of-the-art computational fluid dynamics technique, called LES in case of the flow past an airfoil at a small angle of attack. In the present state of computational fluid dynamics, the computation of the flow is preferred to be carried out on unsteady way. It is well known that for the majority of fluid flow phenomena the classical Reynolds-Averaged Navier-Stokes equation-based modelling does not perform acceptably [1] and [2]. LES is promising, but it still requires unacceptably high computational efforts for modelling the flow even at moderate Reynolds numbers [3], [4] and [5]. By using LES, the flow can be described on a way which is very adequate to the underlying physics, despite of the obligation to use modelling assumption below the grid resolution level. The weak point of LES is the so called sub-grid scale (SGS) model that influences the characteristics of the large, resolved turbulent motions [5] and [3]. Although the most widely used SGS model is the classical Smagorinsky model [6], it is claimed to fail in predicting laminar-turbulent transition. As transition is expected to occur in the present flow, the dynamic Smagorinsky model [7] was used.

Apart from knowing a widely accepted way of modelling the flow in the boundary layer and in the regions of free shear layers, another major factor is present that influences the results orders of magnitudes more than the way of SGS modelling [8] and [9]. This is the resolution of the computational grid [10]. The number of cells in the computational grid is limited by the available computational facility. However, as LES contains a cut-off wave number, below of which, the motion of the flow is modelled and not computed, there is an upper limit in cell number as well. This upper limit obviously depends on the Reynolds number, but it cannot be determined exactly. The purpose generally is to find the grid resolution, above which, the results are not differing from the ones obtained on this resolution. This grid will be appropriate only for a single configuration, i.e. a certain SGS model at a certain Reynolds number for a certain type of geometry. In this paper the grid dependency of the flow characteristics is shown for six different grid resolutions on eight different scenario simulations.

3. Geometry, computational domain and the grids

The geometry of interest is represented in Fig. 1. The airfoil of RAF-6E type is characterized by a flat pressure side (PS) [11], [12]. This airfoil has been already investigated in a previous work [13], where the results of computations were compared to those from experiments. The computed results correlated well with the pressure measurements [14].

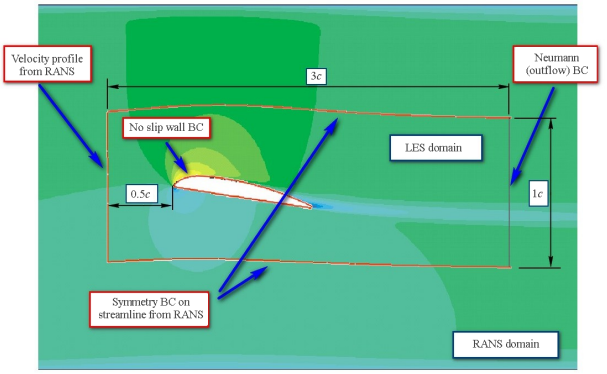

Figure 1: *The LES computational domain with the boundary conditions and the pressure distribution in whole cross section in RANS.*

3.1. Boundary conditions

The LES computations were carried out in a sub-zone of the total flow domain to save up computational cells. The boundary conditions on the boundaries of the sub-zone were determined by means of 2D RANS computations (more advanced techniques are proposed in [16], [17], [18] and [19]). These computations took into account the total flow domain which had a size of $15c$ x $2.5c$ in streamwise and wall-normal direction (details were published in [14]). The airfoil was positioned according to the corresponding wind tunnel measurements which are detailed in [15]. The inlet and outlet boundaries were placed sufficiently far from the airfoil to achieve minimal influence on the flow in the vicinity of the airfoil. Outflow boundary condition was applied. On the outlet. From this simulation, the streamlines have been determined, and two streamlines were considered to be the upper and lower boundaries of the sub-zone. In the spanwise direction periodic boundary condition was applied as can be seen in Fig. 25. The LES domain, i.e. the previously mentioned sub-zone, has the dimension of $3c$ x $1c$. The applied boundary conditions are indicated in Fig. 1.

3.2. The different simulation scenarios

Based on [1], [19] and [20] the domain spanwise width and spanwise grid resolution distribution are not obvious. In present work, the grid resolution and spanwise extension were changed. The different cell number of the case, simulation spanwise extension (L_z), number of spanwise cells (N_z) and important numerical parameters are shown on Table 1. In the case of four in eight case the spanwise extension of domain was fixed at $L_z = 0.5c$.

Seven grids were characterized by constant streamwise resolution but three different spanwise resolutions. In the *LES_05_50_fine* case the streamwise resolution (N_x) was increased for better predicting the flow properties in the region of a laminar separation bubble between $0.2c$ - $0.4c$ as well as in the region of the turbulent boundary layer until the trailing edge.

Three grids can be seen in Fig. 2 with constant spanwise width but different spanwise grid density (*LES_05_100, LES_05_50* and *LES_05_25*). It is visible that the spanwise resolution is refined considerably. More details about the grid is shown in Fig. 3 and Fig. 4.

Table 1: *The grid and numerical parameters.*

Case	N	L_z	N_z	CFL	FTN
LES_0125_50	2006150	0.125	50	0.82	18.4
LES_025_50	2006150	0.25	50	0.231	8.2
LES_05_25	1003075	0.5	25	0.267	13.4
LES_05_50	2006150	0.5	50	0.867	7.3
LES_05_50_fine	2414150	0.5	50	0.243	9.7
LES_05_100	4012300	0.5	100	0.385	7.2
LES_1_50	2006150	1	50	0.877	9.3
LES_1_50_cont	2006150	1	50	0.967	32.4

3.3. Grid details

The domains were meshed using an O-H structure using hexahedron cells, the O type was used for the vicinity of the airfoil (Fig. 3). The grid resolution on the airfoil is 247 grid points (except *LES_05_50_fine* case where there are 353 grid points). For all of the cases the pressure side contains 75 grid points. The mesh was successively refined in the direction to the walls by an expansion ratio of approximately 7% (6.5% - 7.8%) to enable an accurate resolution of the boundary layer. The wall normal size of the first cells around the airfoil increases linearly along the chord both on the suction side (SS) and PS, starting from the leading edge of $10^{-5}c$ increasing to $2 \cdot 10^{-5}c$ at the trailing edge (Fig. 3). This resolution corresponds to cell sizes in wall units (y^+) less than 1 in the case of 99% of the cells. The maximum value of the wall units stays below 1.2 in all cases. The equiangle skewness of none of the cells exceeds 0.67, which is appropriate for the numerical schemes used in this study. The volume ratio of adjacent cells is smaller than 1.25 in the domain.

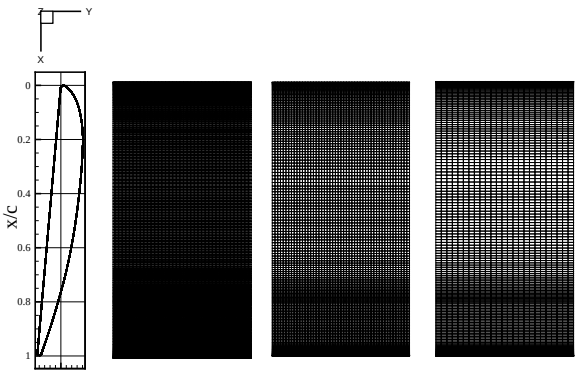

Figure 2: *Three of the investigated grids with $L_z = 0.5c$ constant. Spanwise resolutions are: 100 cells ($N_z = 100$), 50 cells ($N_z = 50$) and 25 cells ($N_z = 25$).*

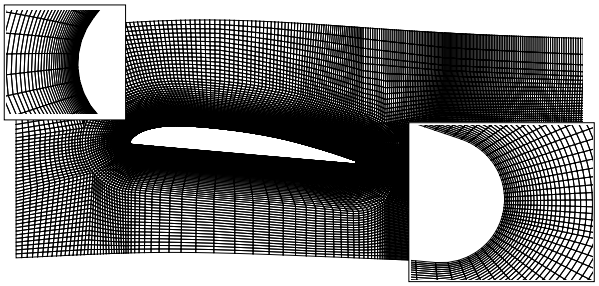

Figure 3: *The grid details in 2D (not in the case of fine).*

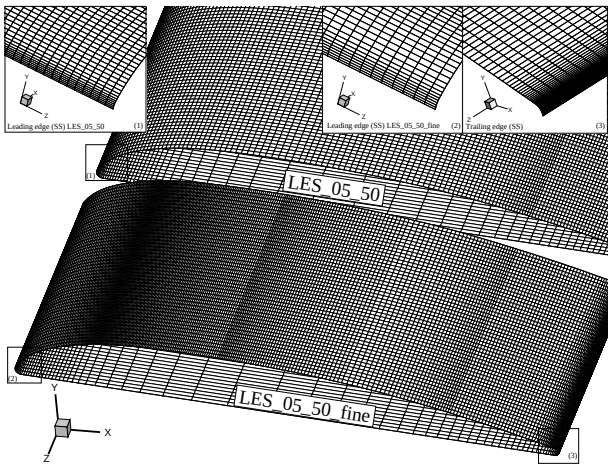

Figure 4: *The grid with details on leading edge of suction side and around the trailing edge (LES_05_50 and LES_05_50_fine).*

4. Solver

In order to calculate the flow field the dynamic Smagorinsky SGS model [7] implemented as [6] was used for the LES. The time step for all of the simulation is set to match the required aerodynamic time resolution, to follow the Courant Friedrichs Lewy (CFL) criteria (Table 1). The LES used explicit filtering [6] to determine the limit of the resolved scales down to the cut-off wave number. The governing equations were discretized on an incompressible way with implicit second-order schemes for the convection and diffusion terms. The equations are solved in the framework of the finite volume method with a collocated variable arrangement provided by the commercial software ANSYS-FLUENT.

To minimize the effect of the spatial discretization error, bounded central differencing scheme (BCD) was adopted for convective terms of the momentum, while the pressure in the momentum equation was discretised with standard first-order scheme. The pressure and velocity coupling in the momentum equation were absolved with the fractional step method (FSM) based on the approximation of factorization. The time discretization was realised with the non-iterative time-advance (NITA) scheme. This scheme was stable during all of the simulation, and it saved approximately the 75% of the time of the simulation in contrast to the iterative time-advance scheme using the inner circle of the iteration.

To characterize the running time, the non-dimensional flow through number (FTN) is introduced. FTN is based on the time needed for a particle of velocity U_{ref} to travel from the inlet of the domain to its outlet. This value is computed as (1).

$$FTN = \frac{t_{flow} U_{ref}}{3c} \tag{1}$$

During the simulation the kinetic energy was monitored (Fig. 6), to monitor the temporal laminar-turbulent transition of the flow in the domain. This evaluation shows the fully developed character of the flow after approximately 1.3 FTN (in the case of *LES_05_50*), when time-averaging was started. Beside this time averaging, spatial averaging was applied in spanwise direction, for further evaluation. This process provides that the results are comparable with measurement data. More details see Section 5.2.1.

5. Effect of grid resolution on the statistical averages, qualitative and quantitative comparison

5.1. Observations along post processing lines

The velocity field validation is based on the six lines being perpendicular (Fig. 5) to the SS surface of the airfoil, and three lines being perpendicular to the streamwise direction in the wake of the airfoil, at $1.1c$, $1.25c$ and $1.5c$ and one being upstream of the airfoil.

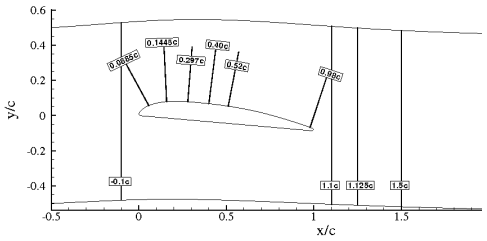

Figure 5: *Postprocessing lines being perpendicular on the SS surface of airfoil at* $-0.1c$*,* $0.0885c$*,* $0.1445c$*,* $0.297c$*,* $0.40c$*,* $0.52c$*,* $0.98c$*,* $1.1c$*,* $1.25c$ *and* $1.5c$*.*

In order to transform the results into the airfoil local coordinate-system, rotation matrix was applied, and the results are presented in *local coordinate-systems*.

The LDA studies provided one component turbulence intensity data, but in the numerical simulation every elements of the Reynolds Stress Tensor (RST) can be calculated.

5.2. The velocity field validation

The postprocessing is based on the fluctuating component of the resolved RST as well as on the streamwise component of the averaged velocity. The instantaneous flow parameters were analysed and the time- and spanwise-averaged results were validated as well. The velocity is normalized by U_{ref} and the RST component is normalized by the U_{ref}^2. The normalization is not note all of in the captions of the figures which contains just the compared name of the cases. Each postprocessing line has its own local coordinate system which is signed by dotted line. The LDA measurements are marked with ■ and are connected with doted lines. Postprocessing results are presented on from Fig. 7 until to Fig. 19, the normalized streamwise velocity, the normalized averaged rms and the rms component. The preliminary results have been shown respectively that the computed velocity profiles underestimate the measurements with the LDA

measurement data downstream the leading edge, upstream the trailing edge and in the wake. This same underestimation were observed in [21], [22], [8] in the wake. Downstream of the transition zone the simulation over predicts the velocity out of the boundary layer. In the case of velocity the comparison is focusing on just the upstream of trailing edge and the wake. The next sub section provides more details about that investigation.

5.2.1. No. 1 scenario, check the convergence of the simulations. Compare LES_1_50 (□) and LES_1_50_cont (▽)

In this comparison we try to judge the simulation time. By the preliminary presumed the approximately 7 FTN is enough for get an acceptable results, but keep in view the length of the simulation because of the time averaging. The simulation time averaging started became stable by on whole domain characterized adequate parameter (kinetic energy) (Fig. 6). In this scenario checked the in the case of *LES_1_50* , while the simulation time 9.3 FTN and *LES_1_50_cont*, while that time was 32.4 FTN.

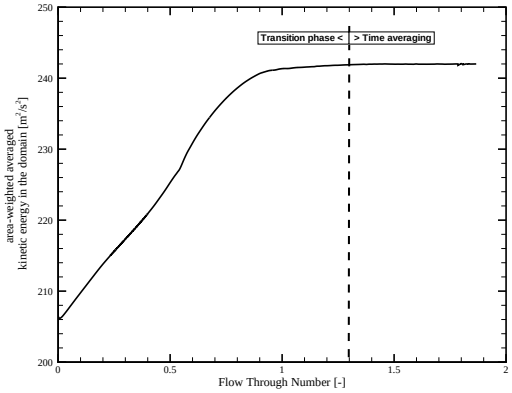

Figure 6: *The simulation convergence check of turbulent kinetic energy in the case of LES_05_50.*

The Fig. 8 did not point significant difference in the aspect of velocity field.Even the magnitude rms values shows minimal, 1.08% (based on the bigger value) different improve the longer averaging time.

The rms component shows a significant difference in v_{rms} at $0.40c$, $0.52c$ and in w_{rms} at $0.52c$. The streamwise components coincidence in both case as well as all the components.

It seems that convergence error is provides the same order of magnitude as the previous examination but this is still smaller than the mesh size deviation. Finally, establish that the minimal 7 FTN simulation time comparable results could be provide. But unfortunately the mesh dependency is exists.

5.2.2. No. 2 scenario, effect the finer grid distribution near the presumable laminar-turbulent transition. Compare LES_05_50 (▲) vs. LES_05_50_fine (▼)

The aim of this comparison to check the effect of the finer grid on close to the transition regime. To compare the velocity-magnitude *LES_05_50* and *LES_05_50_fine* cases, when the nodes are 278 grid nodes of the SS against the original 172 grid nodes there is no significant difference. The rms values does not show a convergent results in this case but it seems that the finer is shown better agreements, but in the results of the rms in the case of $1.25c$ and $1.5c$on are shown huge differences and uncertainty (Fig. 14). In this case this results conditional in the wake. Further simulation run is required to eliminate the uncertainty of results.

5.2.3. No. 3 scenario, the different spanwise grid density effect. Compare LES_05_25 (△), LES_05_50 (▲) and LES_05_100 (○)

In this study the domain width is constant ($L_z = 0.5c$). During this investigation it to be looking for the answer, how the structures are develop and how to be formed the boundary layer.

Simulations in this case are more comparable to the measurements data as the grid density goes to the finest grid density at the $0.98c$ position. The best agreement the *LES_05_100* shows with the measurements. It is corresponding the Fig. 20, as the boundary layer is thickness as the cell number increased. And same tendency is present at the end of the SS, at $0.98c$ (Fig. 7) in the wake still the *LES_05_100* shows the best results.

On the streamwise rms (u_{rms}) can be seen in Fig. 12. Similar tendency can be noticed as it is explained in [8]. The simulation produces better agrement while the grid density increasing. In the wake and at $1.25c$, $1.5c$ shows consequent underestimated differences from the measurements.

In the detailed examination the component of the rms in the transitional region describes the u_{rms} and v_{rms} is the dominant and throughout of the suction side in Fig. 17 as in Fig. 18 as well. In the cross component (w_{rms}) the magnitude is 25% of u_{rms} and the tendency are fit in the case of $0.52c$ and $0.98c$ but turn over at the presumable laminar-turbulent transition. Finally, a well known observation was justifyed.

5.2.4. No. 4 scenario, different domain spanwise width. Compare LES_0125_50 (●), LES_025_50 (■), LES_05_50 (▲) and LES_1_50 (□)

This scenario is try to get answer about the domain width. Fig. 10 is shown the bigger boundary layer than thinner the domain. In two thickest cases (*LES_05_50* and *LES_1_50*) separation have been observed in the boundary layer at the $0.98c$. Similar tendency realized in the magnitude rms (Fig. 15). The domain size change affected by the turbulence anisotropy the fluctuation of the x, y and z velocities which is presented in Fig. 17, Fig. 18 and Fig. 19. Close to the trailing edge all the three components shows the similar sequential decrease tendency as it shows in Fig. 15. After the beginning of the transition ($0.2c$), the streamwise fluctuation is increased with one order of magnitude. The rms of the v_{rms} is smaller than rms of the u_{rms} with one order of magnitude. The thickness of the boundary layer can be also read from Fig. 17 and Fig. 19. The domain reduction is resulted in increase of all normal Reynolds stress components except close to the trailing edge where the trend is the opposite; the production of turbulence in the turbulent part of the SS is enhanced by size reduction but reduced close to the trailing edge. Final conclusion, the smallest width produces the best agreement with the LDA measurements at the trailing edge.

5.2.5. No. 5 scenario, investigation the domain reduction in additional to keep the cell aspect ratio. Compare LES_1_50 (□) vs. LES_05_25 (△)

There is no effect on the boundary layer thickness in this scenario, but the velocity profiles at $0.98c$ are shown minimal more auspiciously agreement with the measurements but the rest of the profiles in the wake there are not shown significant difference (Fig. 11).

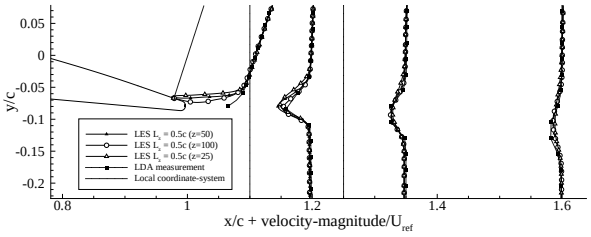

Figure 7: *Case of LES_05_25, LES_05_50 and LES_05_100.*

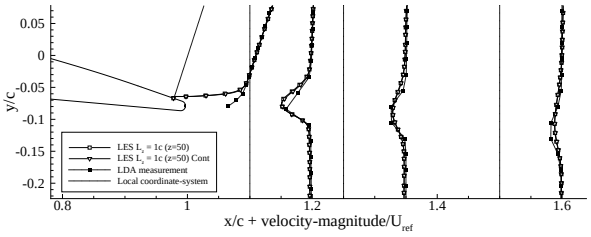

Figure 8: *Case of LES_1_50 vs. LES_1_50_cont.*

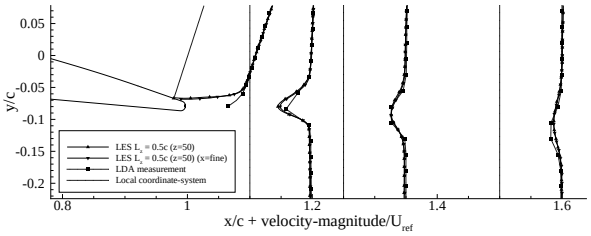

Figure 9: *In the case of LES_05_50 vs. LES_05_50_fine.*

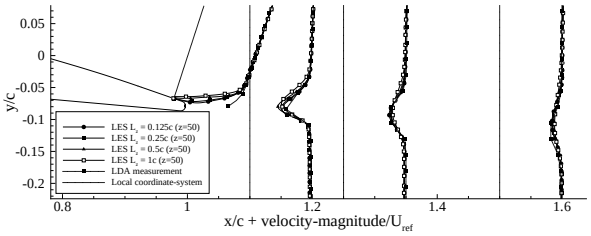

Figure 10: *Case of LES_0125_50, LES_025_50, LES_05_50 and LES_05_1.*

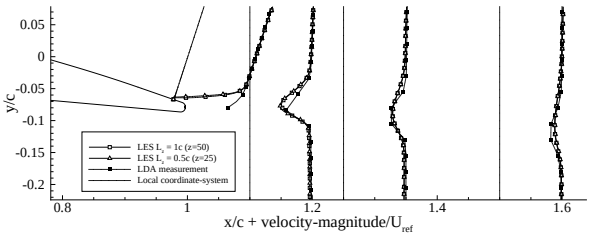

Figure 11: *Case of LES_1_50 vs. LES_05_25.*

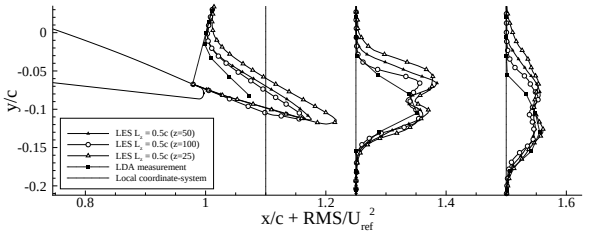

Figure 12: *Case of LES_05_25, LES_05_50 and LES_05_100.*

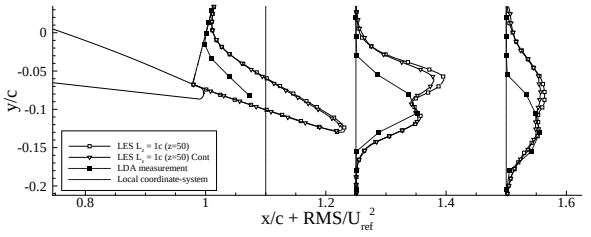

Figure 13: *Case of LES_1_50 vs. LES_1_50_cont.*

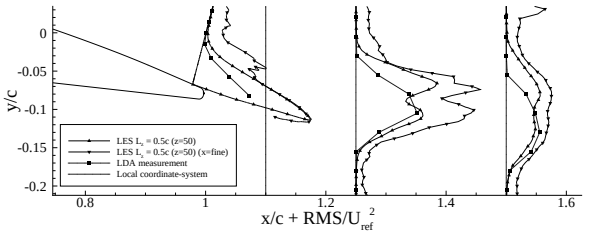

Figure 14: *Case of LES_05_50 vs. LES_05_50_fine.*

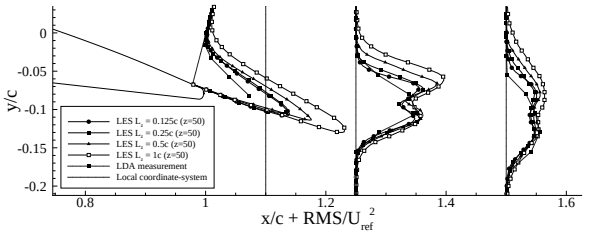

Figure 15: *Case of LES_0125_50, LES_025_50, LES_05_50 and LES_05_1.*

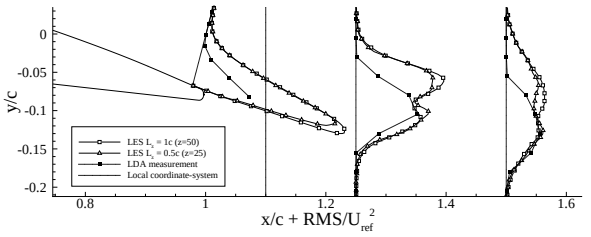

Figure 16: *Case of LES_1_50 vs. LES_05_25.*

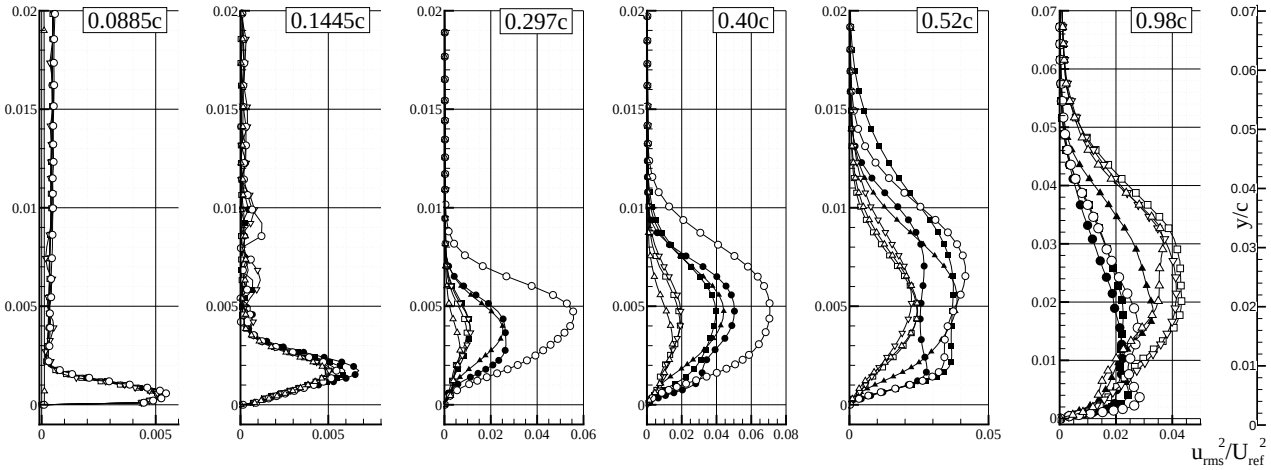

Figure 17: *Normalized streamwise rms (u_{rms}) by U_{ref}^2.*

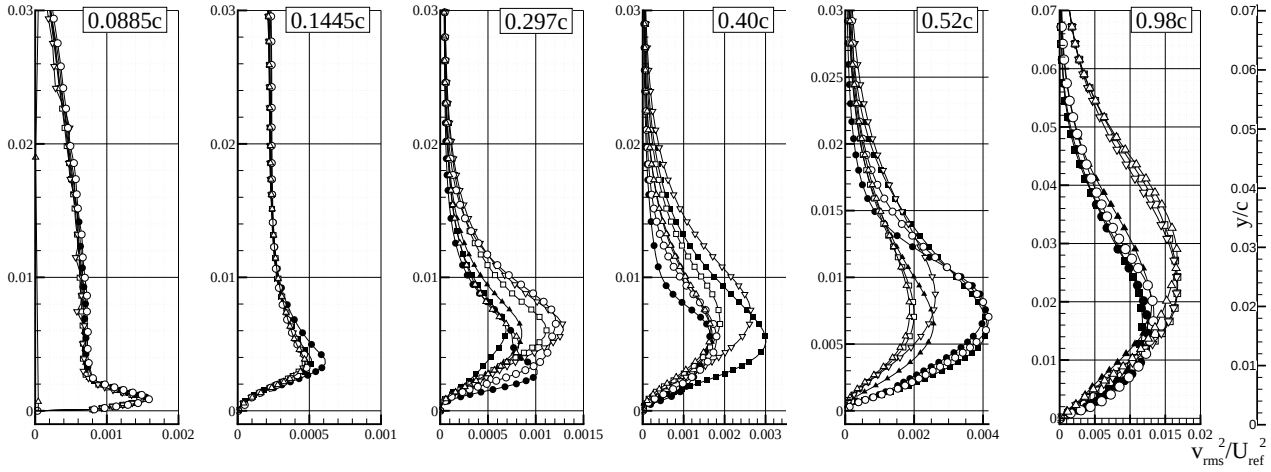

Figure 18: *Normalized cross rms (v_{rms}) by U_{ref}^2.*

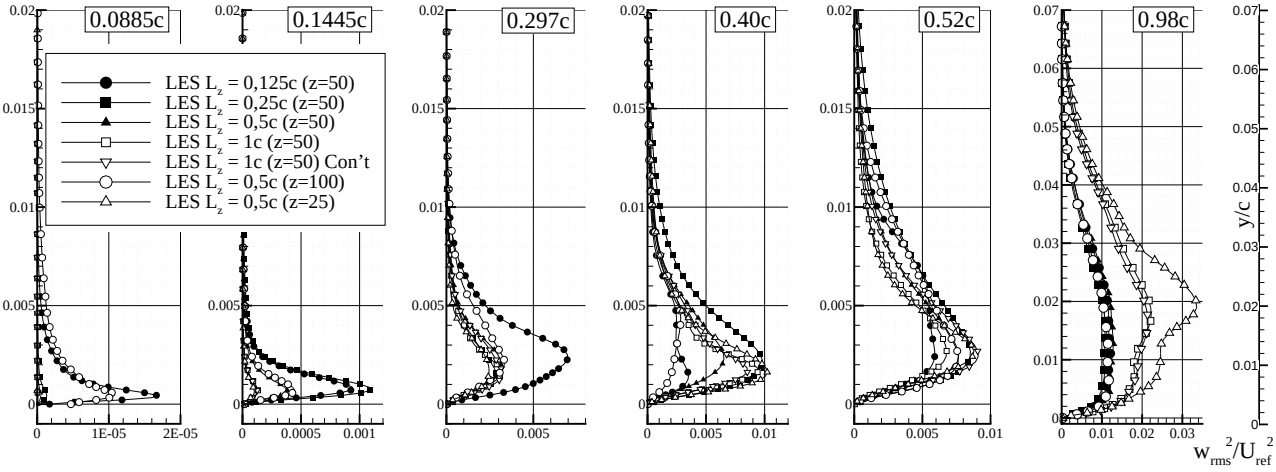

Figure 19: *Normalized cross rms (w_{rms}) by U_{ref}^2.*

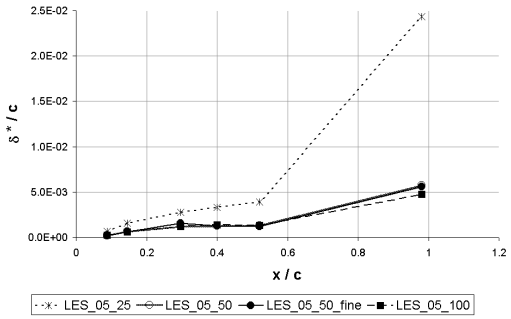

Figure 20: *Displacement thickness on suction side at 0.0885c, 0.1445c, 0.297c, 0.40c, 0.52c and 0.98c.*

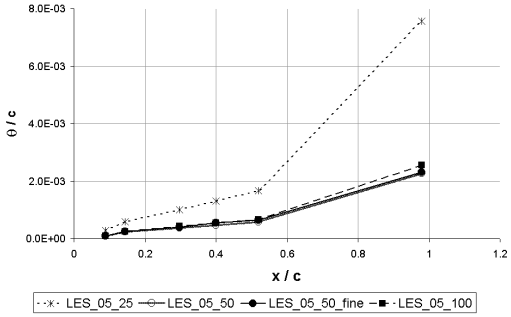

Figure 21: *The momentum thickness on suction side at 0.0885c, 0.1445c, 0.297c, 0.40c, 0.52c and 0.98c.*

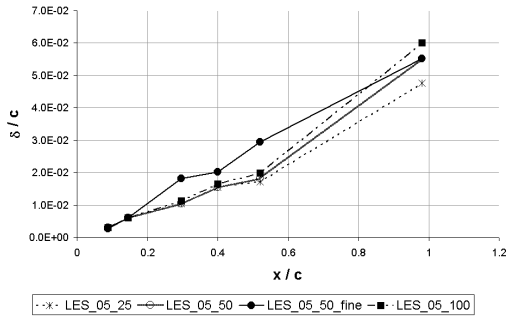

Figure 22: *Boundary layer thickness on suction side at 0.0885c, 0.1445c, 0.297c, 0.40c, 0.52c and 0.98c.*

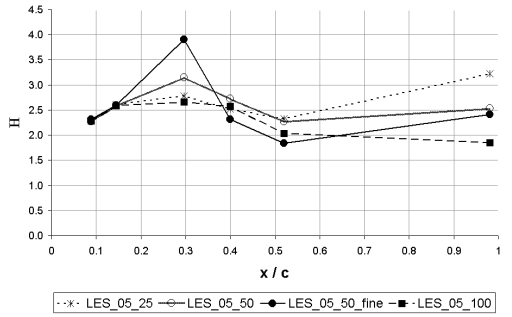

Figure 23: *Shape factor at 0.0885c, 0.1445c, 0.297c, 0.40c, 0.52c, 0.98c.*

In the case of the rms values, the *LES_05_25* is shown a smaller rms peak (Fig. 16), but at $1.25c$ the two peak indifferent nature are shown.
To analyze the rms component it can be conclude that the streamwise (u_{rms}) is the dominant (Fig. 17). The v_{rms} is shown correspondence to the each other the simulations. The w_{rms} is show 0.05%, 0.1%, 0.3% and 1.2% differences $0.297c$, $0.40c$, $0.52c$ and $0.98c$ respectively. While before the transition the both simulation corresponds with each other.

5.3. Observations on SS in rms

The investigation could be divided three part by strainwise direction in the aspest of the rms values. The first part is contain from the stagnation pont and beginning of the transition zone (appr. $0.3c$). All of the rms components is developed in similar way at the beginning, but in the case *LES_0125_50, LES_05_100* and *LES_05_025* 2 order of magnitude bigger w_{rms} values shows between $0 - 0.005$ at y/c than u_{rms} and v_{rms}.
In the second regime therefrom the transition zone until the TE the tendency in all the components of the rms is consequently constant. In the order of *LES_05_25, LES_1_50_cont, LES_1_50, LES_0125_50, LES_05_50, LES_025_50, LES_05_100.* More details you find on scenario sections.
In the last regime at the TE and past the airfoil the tendency is totally turn over again, consequently.

5.4. Integral parameters of the boundary layer

To compare the spanwise grid density effect on the integral parameters, first the momentum and displacement thickness of the boundary layer are determined at different streamwise locations along the central plane of the airfoil section. These values are determined from the statistical average of the velocity field. The displacement $\delta^\star$ (normalized by the chord length) and momentum thickness Θ (normalized by the chord length) were determined from (2) and (3), where *u* is the velocity. The shape factor (*H*) defined in (4) and applied for the airfoil [23]. The shape factor value distribution shows slow increase in the range $0.2c$-$0.4c$, that it shows that the quality is changed in the boundary layer where the measurements and the visualization techniques [13].

$$\delta^\star \doteq \int_0^{y_{umax}} 1 - \frac{u}{u_{max}}\, dy \tag{2}$$

$$\Theta \doteq \int_0^{y_{umax}} \frac{u}{u_{max}} \left(1 - \frac{u}{u_{max}}\right) dy \tag{3}$$

$$H = \frac{\delta^\star}{\Theta} \tag{4}$$

Contrary to the general definition of the momentum and displacement thicknesses [23] here u_{max} is used instead of the free stream velocity. The reason for this choice of reference velocity is the peaky character of the velocity profiles over the surface of the airfoil. It was assumed that the boundary layer ends at the maximum of the velocity profile (Fig. 22). The integrals were carried out by using the trapezoid rule. The evolution of the momentum and displacement thicknesses along the chord of the airfoil can be seen in Fig. 20 and Fig. 21. One can realize that as long as only the spanwise resolution is changed, both the momentum and displacement thicknesses coincide upstream from $0.2c$ of the suction side of the airfoil.

5.5. Qualitative comparison

The change in spanwise resolution leads to only small differences in the thickness values for the coarser streamwise resolved case. The difference due to the change in the spanwise resolution is more apparent towards the trailing edge of the airfoil. The increase in the difference towards the trailing edge indicates that the spanwise resolution plays a significant role. The effect of the resolution on the flow structures towards the trailing edge of the suction side can be seen in Fig. 24 from top view and in Fig. 25 and Fig. 26. The relevant flow structures are vortices, thus they are visualized on the images. For the visualization of the vortices, the Q criterion was used [24] which represents regions where vorticity dominates over the strain rate. The vortical structures originate just downstream the leading edge on the suction side. On the pressure side of the airfoil, the boundary layer stays laminar and there is no vortex formation.

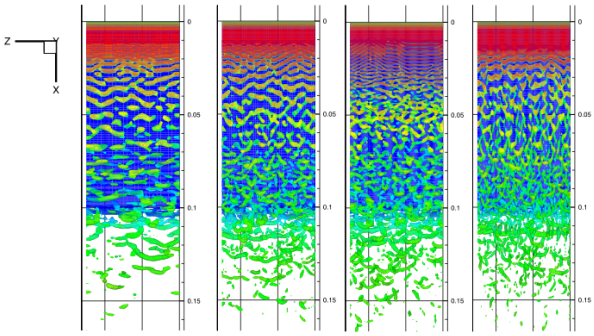

Figure 24: *Grid dependeny through the iso Q at* $5 \cdot 10^5$ *surfaces (LES_05_25, LES_05_50, LES_05_50_fine and LES_05_100).*

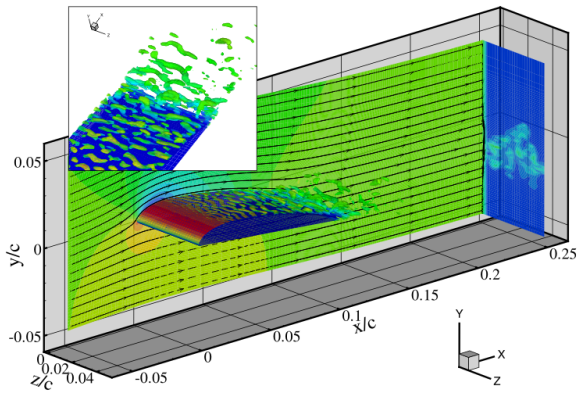

Figure 25: *The iso Q surface at* $5 \cdot 10^5$ *(LES_05_25). On the periodic boundary condition shows the spatial and time averaged static pressure distribution and stream function. The outlet boundary condition shows the instantaneous vorticity*

The structures start to show separate vortex rolls at $0.2c$ Even to analyze the spanwise grid density effect (Fig. 24) shows the grid dependency. At this region it can be seen that the distance between these mainly 2-dimensional rolls is not dependent on the spanwise resolution. However, it strongly depends on the streamwise resolution. It can be observed that in case

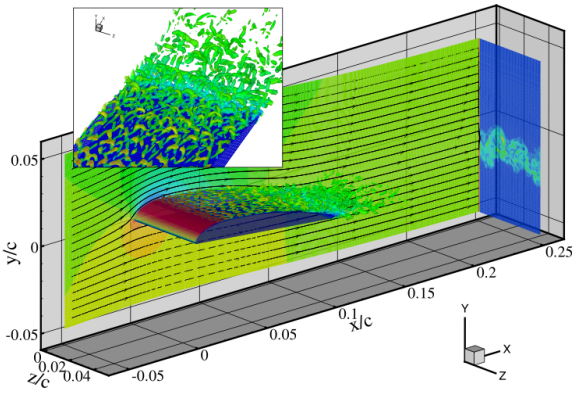

Figure 26: *The iso Q surface at* $5 \cdot 10^5$*(LES_05_100)*

of the same streamwise resolution, the 2-dimensional character of the rolls is stronger for coarse spanwise resolution. In case of the coarsest spanwise resolution, the 2-dimensional rolls reach the trailing edge and are shed into the wake of the airfoil. Even the far wake of the airfoil seems to be more regular, less detailed than in case of finer spanwise resolutions. When the spanwise resolution is increased, the initially 2-dimensional rolls become wavy at a very early development stage and the streamwise orientation of the vorticity begins. At the coarsest spanwise resolution the vortex structure was organized and the vorticity was oriented mainly in the spanwise direction. As the resolution was doubled, the 2-dimensional rolls became unstable and a cascade begun to form. Between *0.5c* and the trailing edge the vortex structures shows a random organization until reaching the trailing edge. In case of the finest spanwise resolution the vortices show an organized structure over the suction side between $0.3c$ and the trailing edge. This region shows the dominance of hairpin vortices [25]. The flow becomes to be random again very close to the trailing edge and small vortex structures are shed into the wake. To summarize the sensitivity of the flow structures on the spanwise resolution, it can be concluded that obviously the details of the flow field are richer for higher resolutions. It has to be noted that also the organization of the structures are different. It means that the overall mechanisms inside the developing boundary layer over the suction surface of the airfoil is significantly changed.

5.6. Cross direction shear stress (τ_z)

Fig. 27 and Fig. 28 show the evaluated spanwise wall shear stress (τ_z) waves on the front part of 1/3 chord of airfoil SS surface, which indicates the transition zone. During the measurements separation was suggested with the flow visualization techniques, but in the case of averaged flow pattern of simulation the separation could not recognized. The separation phenomenon and the transition are the objects of further analysis. The two different colors show negative (darker) and the positive (lighter) values of the shear stress. The shear stress trace is qualitative changed approximately 36%, 38% and 27% respectively *LES_05_25, LES_05_50* and *LES_05_100* by constant domain width (L_z). The nature is permanent but, the structure is changed. The similar effect could be observed narrowing domain (*LES_0125_50, LES_05_50_fine* and *LES_1_50*),

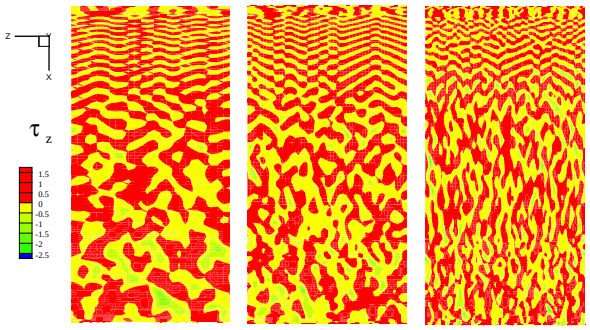

Figure 27: *Instantaneous wall-shear stress in spanwise (τ_z) on the SS (LES_05_25, LES_05_50 andLES_05_100)*

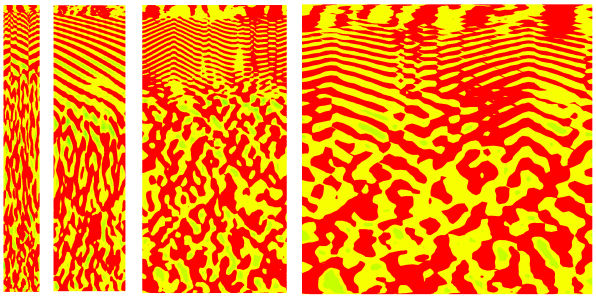

Figure 28: *Instantaneous wall-shear stress in spanwise (τ_z) (LES_0125_50, LES_025_50, LES_05_50_fine and LES_1_50).*

where qualitative change could be realized at approximately 27%, 30% and 46%, respectively. The LES_025_50 case shows different shear stress trace, without any on the break nature on the downstream. Using the experience of the comparison between the velocity, rms and measurements it can be say the approximately 27-28% of the regime is produced realistic results based on the visualization and observation. Further investigation could be focused on the time- and spatial averaged shear stress.

6. Conclusion

The commercially available ANSYS FLUENT was employed in a LES simulation of an airfoil at incidence were conducted, and it was validated with in-house LDA and pressure measurement in NPL type wind tunnel. In this paper we described our observations and results of the cross domain width inestigations. The qualitative validation was realized through oil flow and laser sheet visualization and the separation region on the SS of the airfoil was shown.

Moreover, when cells size were kept in constant to criticize the domain width we found a good agreement in the case of *LES_1_50* and *LES_05_25*. All the cell size investigations we found three regims on the domain; before the transition, before the transition upto the trailing edge and the wake. Evolved tendency in the velocity and its fluctuations were realised.

In this study characteristic structure was reached above the SS of the airfoil. The mesh quality four different aspects were investigated and compareded by; integral parameters of the boundary layer, using the coherent strucure conception, velocity component and normalized fluctuating part with LDA measurements and instantaneous wall-shear stress in different scenarios.

1. The calculated shape factor (H) shows the presumable laminar-turbulent transition zone but this values but it need to be refined. The *LES_05_25* case different Θ and $\delta^\star$ distribution indicated presumably the poor mesh.
2. At higher mesh quality detailed coherent structures and Λ wake were observed.
3. The $L_z = 0.25c$ ($N_z = 50$) and $L_z = 0.5c$ ($N_z = 100$) simulations shown the best agreement with the measurement in the the point of view of the critical simulation at $x = 0.98c$ and in the wake (velocity-magnitude and Reynolds Stress Tensor components).
4. The *LES_05_25* case shows different shear stress (τ_z) distribution as it mentioned in integral parameters and also recognizable the mesh dependency.

7. The CFD facility at BME DFM

The simulations were carried out on the white box HPC cluster of DFM. Which contains 8 cores AMD Athlon64, 10 cores AMD Athlon62x2, 8 cores Intel Core 2 Quad Q6600 and 8 cores Quad-Core AMD Opteron 8350. Simultaneously 4-8 cores were applied. Each computer contains 2, 3 or 16GB. The interconnection Gigabit ethernet connection was realized on Sun Grid Engine Rocks 5.1 operation system.

8. Acknowledgements

This work has been supported by the Hungarian National Fund for Science and Research under contract No. OTKA K63704. This work is related to the scientific program of "Development of quality-oriented and harmonized R+D+I strategy and functional model at BME" project. This project is supported by the New Hungary Development Plan (Project ID: TÁMOP-4.2.1/B-09/1/KMR-2010-0002).

9. List of abbreviations and numenclature

BCD	Bounded central differencing scheme
CFL	Courant Friedrichs Lewy
FSM	Fractional step method
FTN	Flow through number
LDA	Laser-Doppler Anemometer
LES	Large-eddy simulation
NITA	Non-iterative time advanced
PS	Airfoil pressure side
RST	Reynolds stress tensor
SS	Airfoil suction side
SGS	Sub-grid scale
DFM	BME Deaprtment of Fluid Mechanics, http://www.ara.bme.hu
WTL	Theodore von Kármán Wind tunnel Laboratory, http://www.ara.bme.hu/ balczo/karman-wtl/
NPL	National Physics Laboratory

c	chord	$[m]$
L_z	spanwise extension	$[m]$
N_x	number of streamwise cells	$[-]$
N_z	number of spanwise cells	$[-]$
$\delta^\star$	displacement	$[m]$

Θ	momentum thickness	$[m]$
H	shape factor	$[-]$
rms	fluctuations	$[-]$
y^+	wall unit	$[-]$
U_{ref}	inlet reference velocity	$[ms^{-2}]$
ν	kinematic viscosity	$[m^2s^{-1}]$
τ_z	shear stress in cross direction	$[Pa]$

10. References

[1] Davidson, L., Fröhlich, J. and Mellen, C. *LESFOIL: Large Eddy Simulation of Flow Around a High Lift Airfoil* Springer, pp.135-147, 201-222, 2003

[2] Krajnovič, S. and Davidson, L. *Flow around a simplified car, Part 1:Large Eddy Simulation* Journal of Fluids Engineering, Vol. 127, pp 907-918, 2005.

[3] Sagaut, P, Deck, S and Terracol, M. *Multiscale and Multiresolution Approaches in Turbulence* Imperial College Press 2006

[4] Lesier, M, Métias, O. and Comte, P. *Large-Eddy Simulations of Turbulence* Cambridge University Press 2005

[5] Sagaut, P. *Large Eddy Simulation for Incompressible Flows* Springer 2004

[6] Kim, S.E. *Large Eddy Simulation Using Unstructured Meshes and Dynamic Subgrid-Scale Turbulence Models* 34th AIAA Fluid Dynamics Conference and Exhibit, Portland Oregon, 2004

[7] Germano, M, Piomelli, U. Moin, P. and Cabot, W.H. *A Dynamic Subgrid-Scale Eddy Viscosity Model* Physics of Fluids A-Fluid Dynamics, vol 3(7), pp. 1760 - 1765. 1991

[8] Celik, I.B., Cehreli, Z.N. and Yavuz, I. *Index of resolution quality for Large Eddy Simulation* Journal of Fluids Enfineering (127) pp. 949-958, 2005

[9] Guerts, B.J. *Elements of direct and large eddy simulation* Edwards 2004

[10] Tóth, P. and Lohász, M.M. *Anisotropic Grid Refinement Study for LES in Quality and Reliability of Large-Eddy Simulations* ERCOFTAC Series (12) pp. 167-178, 2008

[11] Patterson, G. N. *Ducted Fans. Design for High Efficiency* Australian Council for Aeronautics, Rep. ACA 7 (1944)

[12] *HELIOS Hauptkatalog 2001/2002.* Druckschrift-Nr. 95 178.005 / 03.01

[13] Nagy, L., Lohasz, M.M. and Vad, J. *Hybrid/Zonal RANS/LES computation of an airfoil* In: Proceedings of Sixth Conference on Mechanical Engineering, Gépészet 2008, Budapest, 2008

[14] Nagy, L, Lohasz, M.M. and Vad, J. *RANS simulation of RAF6 airfoil* Proceedings of the Fifth Conference on Mechanical Engineering, Gépészet 2006. Budapest, 2006

[15] Vad, J, Koscso, G, Gutermuth, M, Kasza, Zs., Tabi, T. and Csorgo, T. *Study of the aero-acoustic and aerodynamic effects of soft coating upon airfoil* JSME International Journal Series C-Mechanical Systems Machine Elements and Manufacturing, vol 49(3), pp. 648-656, 2006

[16] Fröhlich, J. and Terzi, D. *Hybrid LES/RANS method for the simulation of turbulent flows* Progress in Aerospace Science (44) pp. 349-377, 2008

[17] Richez, F., Mary, I., Gleize, V. and Basdevant, C. *Near stall simulation of the flow around an airfoil using zonal RANS/LES coupling method* Computer and Fluids (37) pp. 857-866, 2008

[18] Terracol, M. *A zonal RANS/LES appriach for noise source prediction* Flow Tubulence Combust (77) pp. 161-184, 2006

[19] Mathey, F. *Aerodynamical noise simulation of the flow past an airfoil trailing-edge using a hybrid zonal RANS-LES* Computer and Fluids (37) pp. 836-843, 2008

[20] Alam, M. and Sandham, N.D. *Direct numerical simulation of 'short' laminar separition bubbles with turbulent reattachment* J. Fluid Mech. (403) pp. 223-250, 2000

[21] Moreau, S., Neal, D., Khalighi, Y., Wang, M. and Iaccarino, G. *Validation of unstructured-mesh LES of the trailing-edge flow and noise of a Controlled-Diffusion airfoil* Center of Trubulence Research Proceedings of Summer Program 2006

[22] Luo, H., Qiao, W. and Xu, K. *Investigation of mechanisms for separated flow transition control using surface grooves on a high-lift low-pressure turbine profile* hournal power and Energy, Proc. IMeshE (223) pp. 873-886, 2009

[23] Schlichting, H. *Boundary-layer theory* New York: McGraw-Hill, 1955

[24] Hunt, J.C.R., Wray, A.A. and Moin, P. *Eddies,streams, and convergence zones in turbulent flows* Center for Turbulence Research, Annual Research Briefs, pp. 193-202, 1988

[25] Adrian, R.J. *Hairpin vortex organization in wall turbulence* Physics of Fluids (19) 041301 2007